OPEN ACCESS Freely available online

PLOS ONE

Identification and Structural Characterization of a New Three-Finger Toxin Hemachatoxin from *Hemachatus haemachatus* Venom

Vallerinteavide Mavelli Girish[1☯], Sundramurthy Kumar[1☯¤], Lissa Joseph[1], Chacko Jobichen[1], R. Manjunatha Kini[1,2*], J. Sivaraman[1*]

1 Department of Biological Sciences, Faculty of Science, National University of Singapore, Singapore, Singapore, **2** Department of Biochemistry, Medical College of Virginia, Virginia Commonwealth University, Richmond, Virginia, United States of America

Abstract

Snake venoms are rich sources of biologically active proteins and polypeptides. Three-finger toxins are non-enzymatic proteins present in elapid (cobras, kraits, mambas and sea snakes) and colubrid venoms. These proteins contain four conserved disulfide bonds in the core to maintain the three-finger folds. Although all three-finger toxins have similar fold, their biological activities are different. A new three-finger toxin (hemachatoxin) was isolated from *Hemachatus haemachatus* (Ringhals cobra) venom. Its amino acid sequence was elucidated, and crystal structure was determined at 2.43 Å resolution. The overall fold is similar to other three-finger toxins. The structure and sequence analysis revealed that the fold is maintained by four highly conserved disulfide bonds. It exhibited highest similarity to particularly P-type cardiotoxins that are known to associate and perturb the membrane surface with their lipid binding sites. Also, the increased B value of hemachotoxin loop II suggests that loop II is flexible and may remain flexible until its interaction with membrane phospholipids. Based on the analysis, we predict hemachatoxin to be cardiotoxic/cytotoxic and our future experiments will be directed to characterize the activity of hemachatoxin.

Citation: Girish VM, Kumar S, Joseph L, Jobichen C, Kini RM, et al. (2012) Identification and Structural Characterization of a New Three-Finger Toxin Hemachatoxin from *Hemachatus haemachatus* Venom. PLoS ONE 7(10): e48112. doi:10.1371/journal.pone.0048112

Editor: Alejandra Bravo, Universidad Nacional Autonoma de Mexico, Instituto de Biotecnologia, Mexico

Received April 28, 2012; **Accepted** September 19, 2012; **Published** October 29, 2012

Funding: JS acknowledges the funding support from Academic Research Fund (R154000438112). RMK was supported by Bio-Medical Research Council (BMRC - A*STAR). The funders had no role in study design, data collection and analysis, decision to publish, or preparation of the manuscript.

Competing Interests: The authors have declared that no competing interests exist.

* E-mail: dbskinim@nus.edu.sg (RMK); dbsjayar@nus.edu.sg (JS)

☯ These authors contributed equally to this work.

¤ Current address: Scientific Services, Biopolis Shared Facility, Singapore, Singapore

Introduction

Snake venoms are rich sources of biologically active proteins and polypeptides [1]. Apart from its crucial role in paralyzing and digesting prey, snake venom is also an excellent source for novel toxins. Understanding the mechanisms of action of unique toxins, helps in the discovery of novel receptors and in the development of lead therapeutic molecules [2,3]. Snake venom toxins can be broadly categorized as enzymatic and non-enzymatic proteins. They are also classified into various toxin superfamilies. Each superfamily contains structurally similar toxins that exhibit varied pharmacological activities. Some of the well characterized superfamilies of snake venom proteins include three-finger toxins (3FTxs), C-type lectin like proteins (CLPs), phospholipase A_2s (PLA_2s), serine proteases and metalloproteases [4–6]. 3FTxs, non-enzymatic snake venom proteins, are the most abundant toxins found in elapid (cobras, kraits, mambas and sea snakes) and colubrid venoms [4,7]. Besides they have been reported from viperid venoms [8,9]. 3FTxs are composed of 60–74 amino acid residues and 4–5 disulfide bridges. Structurally, all 3FTxs have a stable fold with three β-stranded loops extending from a central core containing all four conserved disulphide bridges, resembling the three fingers of a hand, and hence their common name [10,11]. The conserved cysteine residues, along with invariant residues, such as Tyr25 and Phe27, contribute to proper folding [12]. Some 3FTxs have an additional fifth disulfide in loop I and II as in the case of non-conventional toxins and long-chain neurotoxins, respectively [11,13]. In general, 3FTxs exist as monomers. However, a few of them exist as homo- or hetero-dimers in which the subunits are held together by either non-covalent interactions or by covalent (disulfide) linkages. For example, κ-bungarotoxin [14] and haditoxin [15] exist as non-covalent homodimers where the individual subunits are structurally related to long-chain and short-chain neurotoxins, respectively. The individual subunits are arranged in anti-parallel orientation and are held together mostly by hydrogen bonds between main-chain and side-chain atoms [15–17]. On the other hand, covalently linked 3FTxs include the homodimeric α-cobratoxin (α-CT) [18] and the heterodimeric irditoxin [19]. The structural analysis of the homodimeric α-CT [18] reveals the presence of a β-strand swap as well as two disulfide linkages between loop I of the individual subunits, thereby stabilizing the entire dimeric structure [20]. In irditoxin, the individual subunits are covalently linked through a single disulfide bond between loop I (of irditoxin B) and loop II (of irditoxin A) [19]. 3FTxs also exhibit minor structural variations in the length and conformation of the loops, and

presence of longer C-terminal or N-terminal extensions (for details, see [4]). Despite overall similar fold, 3FTxs recognize a broad range of distinct molecular targets resulting in diverse biological activities [21,22]. Based on their biological properties, 3FTxs can be classified as postsynaptic neurotoxins targeting the nicotinic [23] and muscarinic [24] acetylcholine receptors, cardiotoxins/cytotoxins targeting phospholipid membranes [25], fasciculins targeting acetylcholinesterase (AChE) [26], calciseptins and FS2 toxins targeting L-type calcium channels [27,28], anticoagulants like naniproin, exactin and siamextin [R. M. Kini and colleagues, unpublished data] targeting various coagulation complexes, β-blockers like β-cardiotoxin targeting β_1- and β_2-adrenergic receptors [29], dendroaspin targeting $\alpha_{IIb}\beta_3$ (glycoprotein IIB-IIIa) [30], cardiotoxin A5 targeting $\alpha_v\beta_3$ integrins [31] and antagonists of α_{1A} [32] and α_{2A} [33]adrenergic receptors. The ability of 3FTxs to recognize various molecular targets signifies the need for understanding structure-function relationships of these toxins. The three-finger fold is also observed in various other proteins like xenoxins from *X. laevis* [34] and HEP21 from hen egg white [35], as well as mammalian Ly-6 alloantigens [36], urokinase-plasminogen activator receptor [37] and complement regulatory protein CD59 [38]. 3FTxs in snake venoms are thought to be evolved from non-toxic ancestral proteins through gene duplication and accelerated evolution [39,40].

In continuation of our efforts to understand the relationship between the structure and function of 3FTxs [4,7,15], we isolated, purified and determined the complete amino acid sequence and the crystal structure of a new three-finger toxin (hemachatoxin) from *H. haemachatus* (Ringhals cobra) venom at 2.43 Å resolution. The overall fold of hemachatoxin is similar to other known 3FTxs. The structure and sequence analysis revealed that the fold is maintained by four conserved disulfide bonds. Our efforts on the structure and sequence analyses combined with literature suggested that the unique biological activities of the 3FTxs are associated with the subtle conformational differences in the three β-strand loops. In addition, our analysis suggests that hemachatoxin might be endowed with cardiotoxic/cytotoxic activity.

Results

Isolation and Purification of Hemachatoxin

The *H. haemachatus* crude venom was fractionated on a gel filtration (Superdex 30) column. Peak 3 (Figure 1A) from gel filtration chromatography contained proteins that mostly belong to 3FTx family. Hemachatoxin (*black arrow*) was purified from peak 3 on a C_{18} reverse-phase column (Figure 1B) and further purified to homogeneity using a shallow gradient on the same column (Figure 1C). The homogeneity and mass of hemachatoxin was

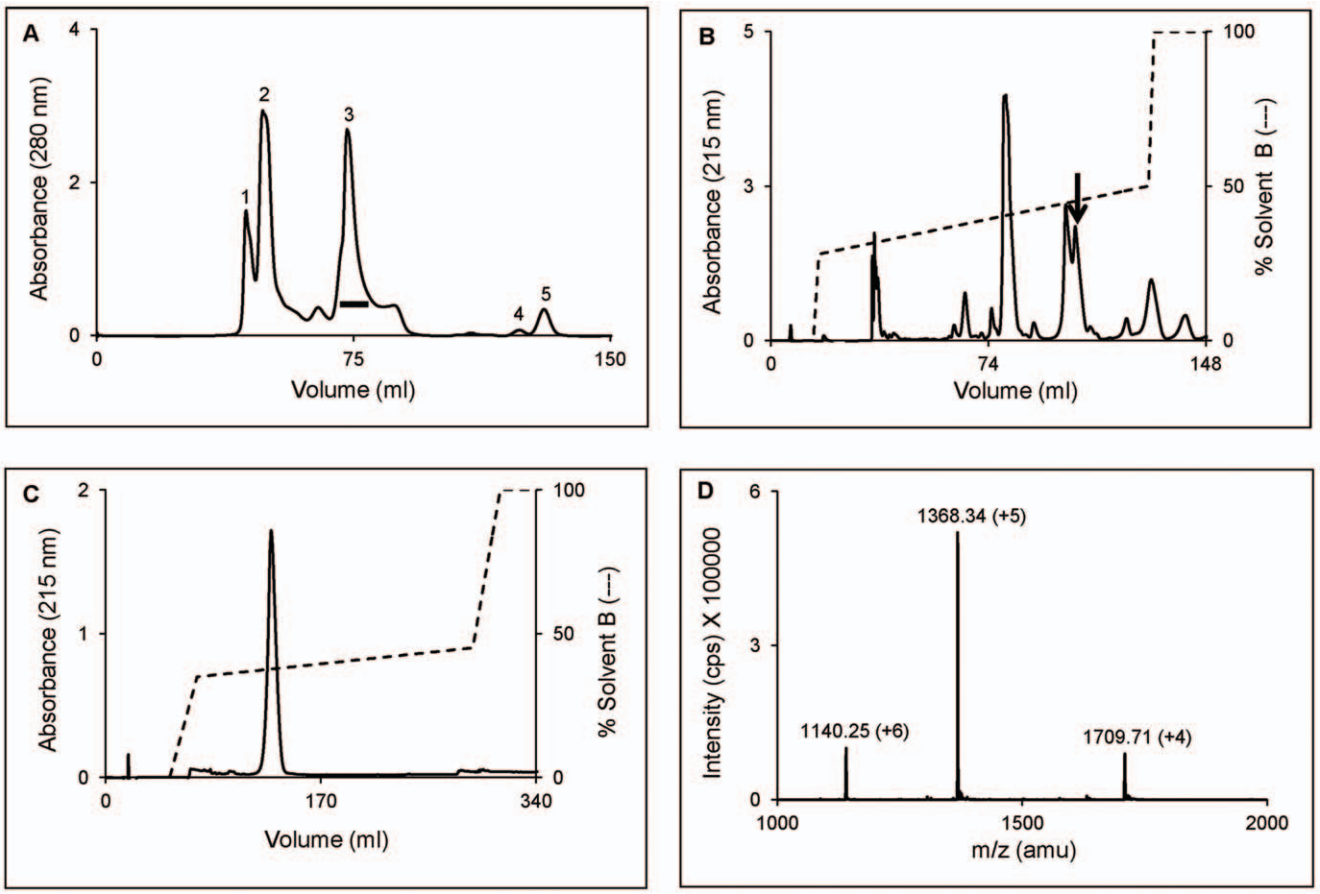

Figure 1. Purification of hemachatoxin from the venom of *H. haemachatus*. (**A**) Size-exclusion chromatogram of the crude venom. The proteins were eluted using 50 mM Tris-HCl, pH 7.4 and monitored at 280 nm. The fractions of peak 3 (*black horizontal bar*) were pooled and sub-fractionated on RP-HPLC. (**B**) RP-HPLC chromatogram of peak 3 using a linear gradient of 28–50% solvent B. The elution was monitored at 215 nm. The *black arrow* indicates the elution of hemachatoxin. (**C**) The re-purification of hemachatoxin on a shallow gradient of 35–45% solvent B. The elution was monitored at 215 nm. (**D**) The ESI-MS profile of hemachatoxin showing the three peaks of mass/charge (m/z) ratio ranging from +4 to +6 charges. The mass of hemachatoxin was determined to be 6835.68±0.94 Da.
doi:10.1371/journal.pone.0048112.g001

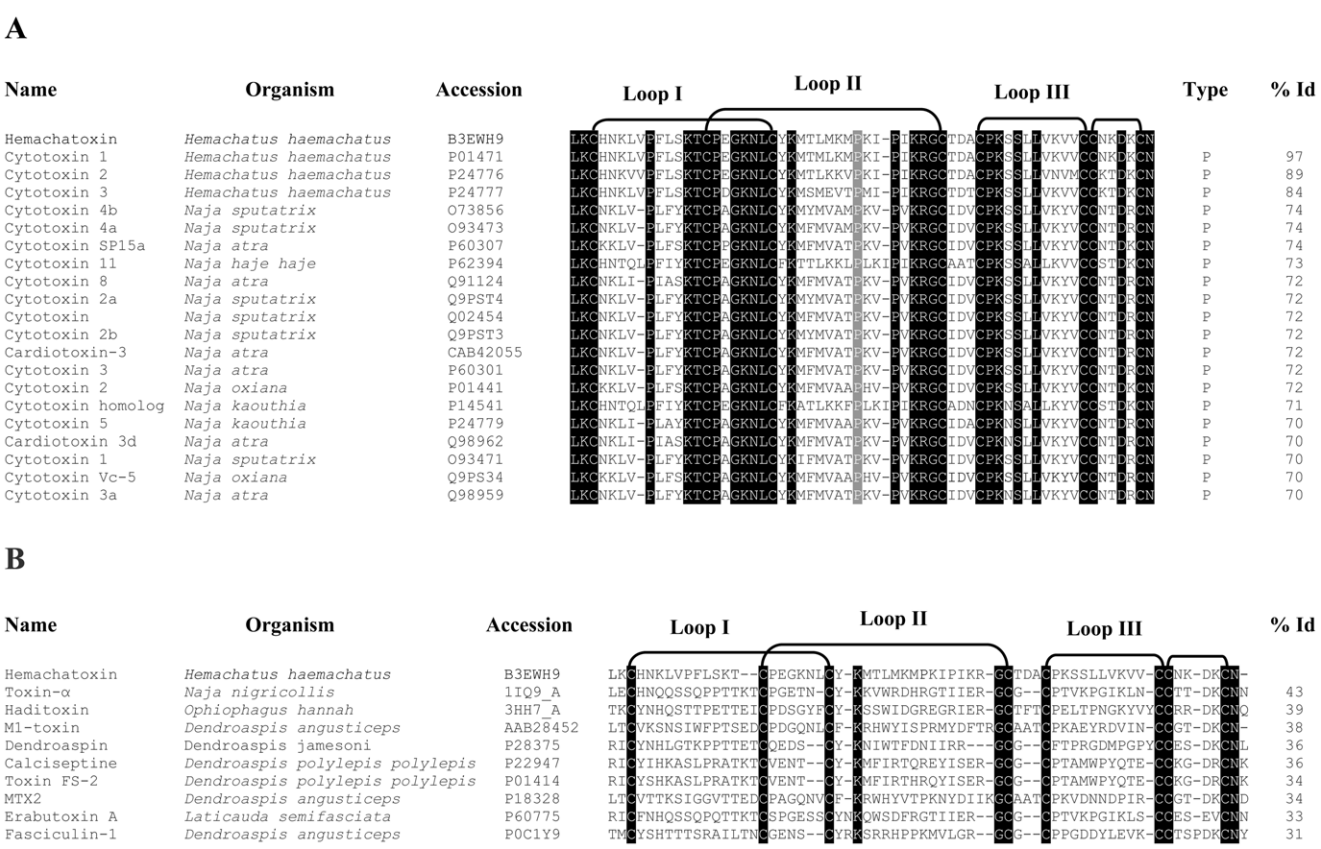

Figure 2. Multiple sequence alignment of hemachatoxin with cardiotoxins/cytotoxins (A) and other three-finger toxins (B). Toxin names, species and accession numbers are shown. Conserved residues in all the sequences are highlighted in black. The type of cardiotoxin based on the conserved Pro31 is highlighted in grey. Disulfide linkages and loop regions are also shown. The sequence identity (in percentage) of each protein with hemachatoxin is shown at the end of each sequence.
doi:10.1371/journal.pone.0048112.g002

determined by electrospray ionization mass spectrometry (ESI-MS). ESI-MS showed 3 peaks of mass/charge (*m/z*) ratio ranging from +4 to +6 charges (Figure 1D). The mass was calculated to be 6835.68±0.94 Da.

Sequence Determination and Analysis

We determined the complete amino acid sequence of hemachatoxin by automated Edman degradation. The first 45 amino acid residues were determined by sequencing the native protein while the remaining sequence was determined from overlapping fragments of chemically-cleaved S-pyridylethylated hemachatoxin (Figure S1A,S1B, S2) (Table S1). The calculated mass of 6836.4 Da from the hemachatoxin sequence agrees well with the experimentally determined molecular mass (6835.68±0.94 Da). The crystal structure (see below) with well defined electron density for the entire hemachatoxin molecule was used to confirm the experimentally determined sequence of the protein as described earlier [41]. The BLAST search [42] showed that hemachatoxin is closely related (>70% identity) to cardiotoxins/cytotoxins, a subgroup of 3FTxs (Figure 2A). Hemachatoxin exhibited highest identity to cytotoxin 1 (97%) [43], cytotoxin 2 (89%) and cytotoxin 3 (84%) [44], purified from *Hemachatus haemachatus* venom. Hemachatoxin differs from cytotoxin 1 [43] in two amino acid positions (Leu27Met28 is replaced by Met27Leu28). This difference was confirmed by ESI-MS (CNBr cleavage site and mass of peptides, Table S1), Edman degradation (Figure S3A, S3B and S3C) and electron density map (see below). Thus hemachatoxin belongs to the 3FTx family based on sequence similarity and the position of cysteine residues (Figure 2).

Structural Analysis

The structure of hemachatoxin was determined by the molecular replacement method using *Naja nigricollis* toxin-γ coordinates (PDB code 1TGX) as a search model. There were two hemachatoxin molecules in an asymmetric unit with each molecule consisting of residues from Leu1 to Asn61 (Figure 3A). Both monomers are well defined in the electron density map (Figure 3B). The model was refined to a final R value of 0.23 (R_{free} = 0.28) (Table 1). The stereochemical parameters of the model were analyzed by PROCHECK [45] and all residues are in the allowed regions of the Ramachandran plot. Each monomer of the asymmetric unit consists of 6 anti-parallel β-strands (β2 ↓ β1 ↑ β4 ↓ β3 ↑ β6 ↓ β5 ↑) that form two β-sheets (Figure 3A). The first β-sheet consists of two anti-parallel β-strands, β1 (Lys2-Lys6) and β2 (Phe10-Thr14), while the second contains four anti-parallel strands, β3 (Leu21-Thr26), β4 (Ile35-Thr40), β5 (Ala42-Ser47) and β6 (Lys51-Asn56). The fold of hemachatoxin is maintained by four disulfide bonds, and these cysteines are strictly conserved among the 3FTxs. The three fingers of hemachatoxin consist of the secondary structures β1Ωβ2, β3Ωβ4 and β5Ωβ6 (Figure 3A). The electrostatic surface representation shows that loops I and II are predominantly charged residues, whereas loop III is highly hydrophobic in nature (Figure 3C). The sequence alignment revealed the conserved

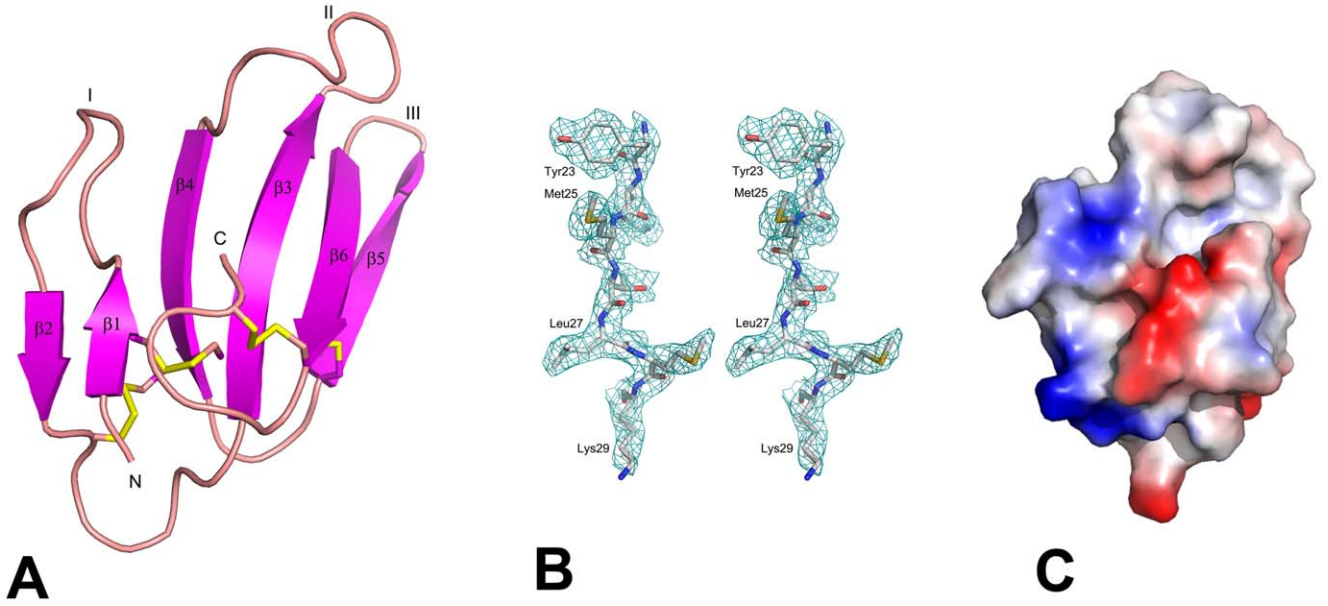

Figure 3. Structure of hemachatoxin. (**A**) Ribbon representation of the hemachatoxin monomer. Cysteine bonds are shown in *yellow*. β-strands, N- and C- terminals are labeled. (**B**) Electron density map**.** A sample final *2Fo-Fc* map of hemachatoxin shows the region from Tyr23 to Lys29. The map is contoured at a level of 1σ. (**C**) The electrostatic surface potential of hemachatoxin is shown in the same orientation as Figure 3A. Blue indicates positive potential and red indicates negative potential in units kT/e. All the structure related figures of this paper were prepared using the program PyMol [77].
doi:10.1371/journal.pone.0048112.g003

residues of hemachatoxin as well as its identity to cardiotoxins/cytotoxins (Figure 4A). Also, hemachatoxin shared the common three-finger fold and molecular shape when compared to its structural homologues (Figure 4B) [46].

Discussion

The three-dimensional structures of snake venom 3FTxs, particularly that of neurotoxins [15,20,47,48] and cardiotoxins/cytotoxins [49–52] have been extensively studied. Here we report the structural characterization of a new 3FTx, hemachatoxin from the venom of *H. haemachatus*. The structural analyses indicate that hemachatoxin belongs to cardiotoxin/cytotoxin subgroup of 3FTx family. It exhibited 97% sequence identity to cytotoxin 1 [43], whose crystal structure has not been determined. ESI-MS, Edman degradation and crystal structure data indicates that hemachatoxin differs from cytotoxin 1 in two amino acid positions (Leu27Met28 is replaced by Met27Leu28) and hence are isoforms. Multiple isoforms of 3FTxs are known to be present in single snake venom [53,54].

As mentioned in the introduction section, 3FTxs, including hemachatoxin, share overall structural similarity (Figure 4B), but they differ from each other in their biological activities. Subtle variations in the size and conformation of β-sheet loops dictate the biological specificities in 3FTxs. For example, the well characterized long-chain (e.g. α-cobratoxin, α-bungarotoxin) and short-chain (e.g. erabutoxin a, toxin-α) neurotoxins that differ in loop size and length of C-terminal extension, exhibit distinct specificity for nAChR subtypes. Short-chain neurotoxins has a longer loop I (12–13 amino acid residues (aa) vs. 9–12 aa in long-chain neurotoxins), a shorter loop II (15–16 aa vs. 19–20 aa in long-chain neurotoxins) and C-terminal tail (2 aa vs. 7–24 aa in long-chain neurotoxins) when compared to long-chain neurotoxins. This longer loop I of short-chain neurotoxins contains key functional residues that are important for recognizing the nicotinic acetylcholine receptor [55,56], while shorter loop I of long-chain neurotoxins lacks these functional residues. The long C-terminal tail appears to 'substitute' for the loop I functional residues and contribute to the receptor binding [57,58]. The deletion of this C-terminal tail reduces the binding affinity [59,60]. Similarly, the difference in the conformations of the three loops appears to dictate the biological specificities of these neurotoxins. Both short-chain and long-chain neurotoxins exhibit equi-potency towards muscle αβγδ nAChR [56,60] but only long-chain neurotoxins, not short-chain neurotoxins, bind to neuronal α7 nAChR with high affinity [61,62]. Detailed structure-function studies indicate that the presence of the fifth disulfide bond in loop II enables long-chain neurotoxins to recognize α7 nAChR. The short helical segment formed by the fifth disulfide is thought to be crucial for the target receptor recognition [62,63]. Thus, size and conformation of the loops indeed affects the interaction of neurotoxins with their receptor. Similarly, structures of loop I in fasciculin [64], and loop III in FS2 [65] and dendroaspin [66] have distinct conformations. Hence, subtle conformational differences in the loops of 3FTxs may help in identifying putative functions.

Hemachatoxin shows highest similarity to P-type cardiotoxins [67] (Figure 2A). Similar to these P-type cardiotoxins, hemachatoxin has the conserved Pro31 and cytolytic site. The three-dimensional structure is similar to P-type cardiotoxins (Figure 4B) (RMSD values, 0.8 to 2.1 Å for 58 to 60 Cα atoms; Z score values, 12.2 to 9.8). Besides, hemachatoxin shows considerable structural identity with S-type cardiotoxins (RMSD 1.1 to 2.8 for 58 to 59 Cα atoms; Z score values, 10.5 to 6.3) (data not shown). However, the similarity with other groups of 3FTxs, such as neurotoxins, muscarinic toxins, fasciculin, FS2 or dendroaspin, is relatively low (Figure 2B, Table 2). The P-type cardiotoxins bind to phospholipids and perturb the membrane surface with their lipid binding sites (6–13, 24–37 and 46–50 amino acid positions in the tip of loop I, II and III, respectively) [67–69]. These hydrophobic residues flanked by cationic residues form cytolytic region in

Table 1. Crystallographic data and refinement statistics.

Data collection*	
Unit Cell (Å)	a = 49.7, b = 50.1, c = 57.8
Resolution range (Å)	50-2.43 (2.47-2.43)
Wavelength (Å)	1.5418
Observed reflections	28936
Unique reflections	5614
Completeness (%)	96.2 (84.5)
Redundancy	3.9 (3.7)
[a]R_{sym}	0.06 (0.17)
I/SigI	20.6 (11.7)
Refinement	
Resolution range (Å) I>σ(I)	30–2.43
[b]R_{work}	0.23
[c]R_{free}	0.28
Root mean square deviation	
Bond lengths (Å)	0.008
Bond angles (°)	1.377
Average B-factors (Å^2)	
Protein atoms (938 atoms)	40.30
Water molecules (62 atoms)	37.1
Wilson B value	36.54
Ramachandran statistics	
Most favored regions (%)	98.31
Allowed regions (%)	1.69
Disallowed regions (%)	0

Statistics from the current model.
[a]$R_{sym} = \Sigma|I_i - \langle I \rangle| / \Sigma|I_i|$ where I_i is the intensity of the i^{th} measurement, and $\langle I \rangle$ is the mean intensity for that reflection.
[b]$R_{work} = \Sigma|F_{obs} - F_{calc}| / \Sigma|F_{obs}|$ where F_{calc} and F_{obs} are the calculated and observed structure factor amplitudes, respectively.
[c]R_{free} = as for R_{work}, but for 10.0% of the total reflections chosen at random and omitted from refinement.
*Values in the parenthesis are the highest resolution bin values.
doi:10.1371/journal.pone.0048112.t001

cardiotoxins [70,71]. We compared the B values of the cardiotoxin loops with those of hemachatoxin. All three loops in P-type cardiotoxins showed a high B value (an increase of 5–8 Å^2) compared with the rest of the molecule. A similar increase in B values (upto 8 Å^2 increase) was also observed in hemachatoxin loops. Only loop II has the crystal contact suggesting that the observed increase in B values might be limited by the symmetry contacts. Nonetheless this analysis suggests that loop II is flexible and may remain flexible until its interaction with membrane phospholipids. These structural analyses also suggest that hemachatoxin might be having cardiotoxic/cytotoxic activity and our future experiments will be directed to characterize the activity of hemachatoxin.

Conclusion

In summary we report the isolation, purification and structural characterization of a new 3FTx, hemachatoxin from *H. haemachatus* venom. The structural and sequence analysis reveals hemachatoxin to be a P-type cardiotoxin. Close comparison of the loops of hemachatoxin with other 3FTxs suggests that hemachatoxin has structural features similar to the well characterized cardiotoxins. The structural analysis combined with literature predicts hemachatoxin to have cardiotoxic/cytotoxic properties. Additional experiments are required to fully characterize the activity of hemachatoxin.

Materials and Methods

Protein Purification

Lyophilized *H. haemachatus* crude venom was purchased from South African Venom Suppliers (Louis Trichardt, South Africa). Size-fractionation of the crude venom (100 mg in 1 ml of distilled water) was carried out on a Superdex 30 gel-filtration column (1.6×60 cm) pre-equilibrated with 50 mM Tris-HCl buffer (pH 7.4). The proteins were eluted with the same buffer using an ÄKTA purifier system (GE Healthcare, Uppsala, Sweden). Peak 3 from the gel-filtration chromatography was sub-fractionated by reverse phase–high performance liquid chromatography (RP-HPLC) on a Jupiter C_{18} column (10×250 mm) equilibrated with solvent A (0.1% TFA). The bound proteins were eluted using a linear gradient of 28–50% solvent B (80% acetonitrile in 0.1% TFA). The mass of each fraction were analyzed on a LCQ Fleet^{TM} Ion Trap LC/MS system (Thermo Scientific, San Jose, USA). Xcalibur^{TM} 2.1 and ProMass deconvolution 2.8 software were used, respectively, to analyze and deconvolute the raw mass data. The peak corresponding to hemachatoxin was pooled and re-chromatographed using a shallow gradient of 35–45% solvent B on the same column. The mass and homogeneity of purified hemachatoxin was analyzed as described above.

Sequencing

Hemachatoxin (1.2 mg) was dissolved in 500 µl of denaturation buffer (130 mM Tris-HCl pH 8.5, 1 mM EDTA, 6 M guanidine HCl). After the addition of the reducing agent β-mercaptoethanol (1.23 µl; 25×molar excess of disulfide bonds), the reaction mixture was incubated under a nitrogen stream for 3 h at room temperature. Subsequently, the alkylating reagent 4-vinylpyridine (5.7 µl; 3×molar excess of β-mercaptoethanol) was added and incubated under a nitrogen stream for another 2 h at room temperature. The S-pyridylethylated protein was immediately separated from the reaction mixture by RP-HPLC on a Jupiter C_{18} column (4.6×250 mm) using a linear gradient of 20–60% solvent B and the mass was determined by ESI-MS as discussed above. For cyanogen bromide (CNBr) cleavage, the S-pyridylethylated protein (0.82 mg) was dissolved in 410 µl of 70% TFA to which CNBr (67.7 µl in 70% TFA) was added in order to yield a final protein concentration of 1 µg/µl. CNBr was used at a molar ratio to methionine residue of 200:1. The reaction tube was incubated in complete darkness for 24 h at room temperature. After 24 h, 8.2 ml of Milli-Q water (10× of reaction mixture) was added into the reaction tube and, subsequently, the reaction tube was lyophilized overnight [72]. The lyophilized sample was re-solubilized in 3 ml of 0.1% TFA for separation by reverse-phase chromatography on a Jupiter C_{18} column (4.6×250 mm) using a linear gradient of 10–50% solvent B. The masses of the peptide fragments were determined by ESI-MS (data not shown). The N-terminal sequence of native hemachatoxin and peptides generated by CNBr cleavage (identified by mass spectrometry data) were determined by automated Edman degradation using a PerkinElmer Life Sciences Model 494 pulsed liquid-phase sequencer (Procise, Foster City, USA) with an on-line Model 785A phenylthiohydantoin-derivative analyzer. The complete amino

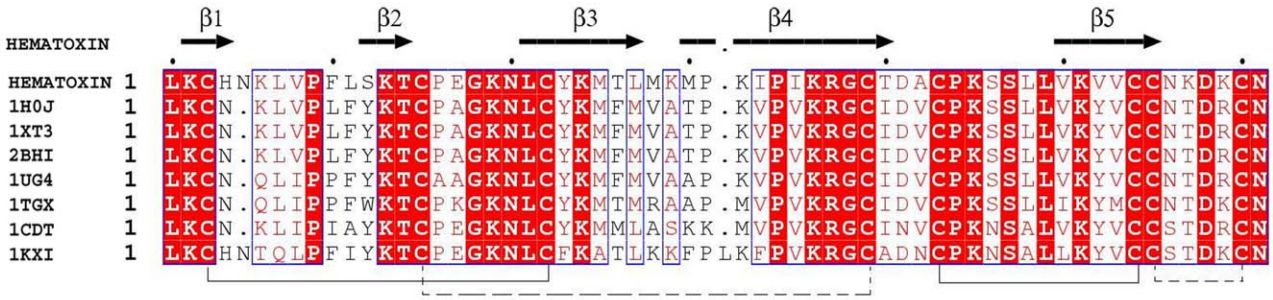
β1
β2
β3
β4
β5
HEMATOXIN
HEMATOXIN 1 LKCHNKLVPFLSKTCPEGKNLCYKMTLMKMP.KIPIKRGCTDACPKSSLLVKVVCCNKDKCN
1H0J 1 LKCN.KLVPLFYKTCPAGKNLCYKMFMVATP.KVPVKRGCIDVCPKSSLLVKYVCCNTDRCN
1XT3 1 LKCN.KLVPLFYKTCPAGKNLCYKMFMVATP.KVPVKRGCIDVCPKSSLLVKYVCCNTDRCN
2BHI 1 LKCN.KLVPLFYKTCPAGKNLCYKMFMVATP.KVPVKRGCIDVCPKSSLLVKYVCCNTDRCN
1UG4 1 LKCN.QLIPPFYKTCAAGKNLCYKMFMVAAP.KVPVKRGCIDVCPKSSLLVKYVCCNTDRCN
1TGX 1 LKCN.QLIPPFWKTCPKGKNLCYKMTMRAAP.MVPVKRGCIDVCPKSSLLIKYMCCNTDKCN
1CDT 1 LKCN.KLIPIAYKTCPEGKNLCYKMMLASKK.MVPVKRGCINVCPKNSALVKYVCCSTDRCN
1KXI 1 LKCHNTQLPFIYKTCPEGKNLCFKATLKKFPLKFPVKRGCADNCPKNSALLKYVCCSTDKCN

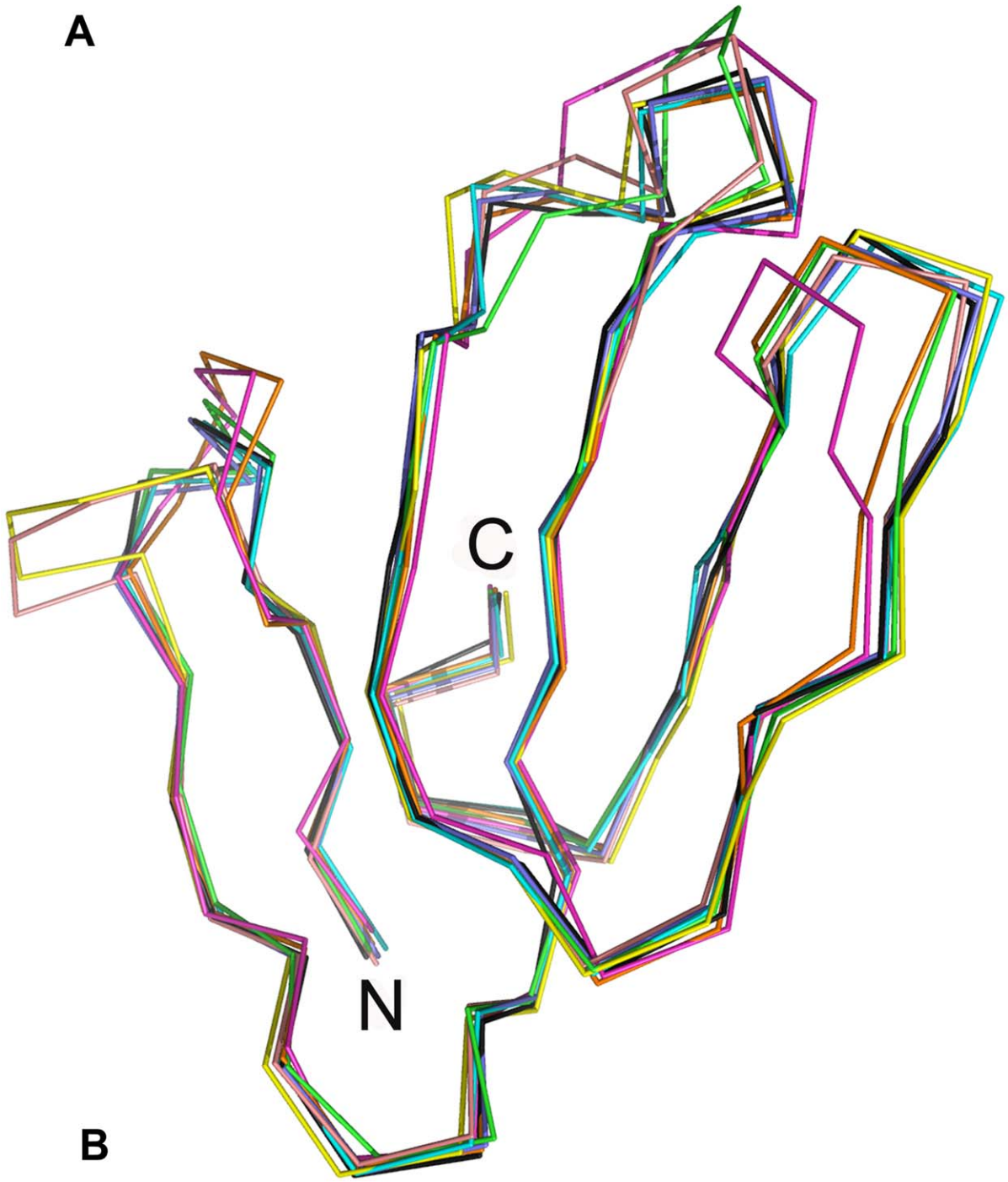
A
C
N
B

Figure 4. Comparison of hemachatoxin with other three-finger toxins. (**A**) Structure based sequence alignment of hemachatoxin and its homologs, cardiotoxin 3 (1H0J), cytotoxin 3 (1XT3), cardiotoxin A3 (2BHI), cardiotoxin VI (1UG4) and cardiotoxin V (1KXI), (all from *Naja atra*), cardiotoxin $V_{II}4$ (1CDT) from *Naja mossambica* and toxin-γ (1TGX) (a cardiotoxin from *Naja nigricollis*). This figure was generated using the programs ClustalW [78] and ESPript [79]. (**B**) Comparison of hemachatoxin with its structural homologs. Hemachatoxin (brown), cardiotoxin 3 [1H0J] (cyan), cytotoxin 3 [1XT3] (black), carditotoxin A3 [2BHI] (blue), cardiotoxin VI [1UG4] (red), cardiototoxin V [1KXI] (pink), cardiotoxin $V_{II}4$ [1CDT] (green) and toxin-γ [1TGX] (yellow).
doi:10.1371/journal.pone.0048112.g004

Table 2. Structural similarity of hemachatoxin with 3FTxs.

Protein	Source	PDB	RMSD*	Z score	Reference
Cardiotoxin V	*Naja atra*	1KXI	1.1 Å(60)	12.2	[49]
Cardiotoxin A3	*Naja atra*	2BHI	0.8 Å(59)	12.0	[50]
Cardiotoxin 3	*Naja atra*	1H0J	0.9 Å(59)	11.7	[51]
Cytotoxin 3	*Naja atra*	1XT3	0.8 Å(59)	11.6	[80]
Toxin-γ	*Naja atra*	1TGX	1.6 Å(59)	11.1	[52]
Cardiotoxin VI	*Naja atra*	1UG4	1.8 Å(59)	11	[81]
Cardiotoxin $V_{II}4$	*Naja atra*	1CDT	1.1 Å(58)	10.5	[82]
Cytotoxin 2	*Naja naja oxiana*	1CCQ	2.1 Å(59)	9.8	[83]
Muscarinic M1 toxin	*Dendroaspis angusticeps*	2VLW	2.4 Å(55)	9.1	[84]
Haditioxin	*Ophiophagus hannah*	3HH7	2.4 Å(58)	8.5	[15]
α-bungarotoxin	*Bungarus multicinctus*	2QC1	2.4 Å(58)	8.4	[85]
Erabutoxin A	*Laticauda semifasciata*	3ERA	2.3 Å(56)	7.9	[86]
Fasciculin 2	*Dendroaspis angusticeps*	1FSC	2.3 Å(55)	7.5	[87]
Toxin FS2	*Dendroaspis polylepis polylepis*	1TFS	2.9 Å(56)	7.4	[65]
Dendroaspin	*Dendroaspis jamesoni kaimosae*	1DRS	3.5 Å(49)	3.6	[66]

*Number of Cα atoms superimposed given in the parenthesis.
doi:10.1371/journal.pone.0048112.t002

acid sequence of hemachatoxin was determined by overlapping sequences.

Crystallization and Structure Determination

Crystallization screens were performed with the hanging drop vapor diffusion method using Hampton Research and Jena Bioscience screens. The protein was at a concentration of 35 mg/ml, and 1:1 crystallization drops were set up with the reservoir solution. The diffraction quality crystals of hemachatoxin were obtained from a reservoir solution containing 150 mM ammonium acetate, 100 mM sodium acetate (pH 4.6) and 25% polyethylene glycol 4000. Crystals were grown up to 10 days and were cryo-protected with 20% (w/v) glycerol supplemented (the mother liquor concentration was maintained by exchanging water with glycerol) with the crystallization condition. Hemachatoxin crystal diffracted up to 2.43 Å resolution and belongs to $P2_12_12_1$ space group. A complete data set was collected using an R-Axis IV^{++} image plate mounted on a rotating anode Rigaku X-ray generator. The data set was processed and scaled using HKL2000 [73]. The structure of hemachatoxin was determined by the molecular replacement method using the program Phaser [74]. The coordinates of *Naja nigricollis* toxin-γ monomer structure (PDB code 1TGX; sequence identity 67%) were used as a search model. The structure solution was obtained with LLG- 94; and TFZ score of 12.3 and RFZ score 4.5. Initial rigid body refinement gave R_{work} 36.6 (R_{free} 43.5). There were two hemachatoxin molecules located in the asymmetric unit. The resultant electron density map was of good quality. Several cycles of model building/refitting using the program Coot [75], and alternated with refinement using the program Phenix [76], lead to the convergence of R-values (Table 1). Non-crystallographic symmetry (NCS) restraints were used throughout the refinement process.

Accession Numbers

The protein sequence data reported in this paper will appear in the UniProt Knowledgebase under the accession number B3EWH9. The three dimensional coordinates and structure factors of hemachatoxin were deposited in the RCSB (www.pdb.org) database with the access code 3VTS.

Supporting Information

Figure S1 Reduction and pyridylethylation of hemachatoxin. (A) The S-pyridylethylated hemachatoxin (*black arrow*) was purified on a linear gradient of 20–60% solvent B. **(B)** The ESI-MS profile of S-pyridylethylated hemachatoxin showing the four peaks of mass/charge (m/z) ratio ranging from +4 to +7 charges. The mass was determined to be 7685.12±1.14 Da.
(TIF)

Figure S2 Separation of peptides derived from cyanogen bromide cleavage of the S-pyridylethylated hemachatoxin on RP-HPLC. A linear gradient of 10–50% solvent B was used. The peptides A and B were sequenced by Edman degradation method.
(TIF)

Figure S3 Chromatographic profiles of PTH-amino acid (phenylthiohydantoin-amino acid) residues 27 and 28 of the Edman degradation cycles 29 and 30. (A) Elution profile of standard PTH-amino acid residues**. (B)** Cycle 29 of Edman degradation showing the 27th residue, PTH-L. PTH-T and PTH-M denotes the carryover from 28th and 27th cycle, respectively. **(C)** Cycle 30 of Edman degradation showing the 28th residue, PTH-M. PTH-L denote the carryover from 29th cycle.
(TIF)

Table S1 The sequence determination of hemachatoxin.
(DOC)

Author Contributions

Conceived and designed the experiments: JS RMK. Performed the experiments: VMG SK LJ CJ. Analyzed the data: JS RMK VMG CJ. Contributed reagents/materials/analysis tools: JS RMK. Wrote the paper: JS RMK VMG CJ.

References

1. Dufton MJ (1993) Kill and cure: the promising future for venom research. Endeavour 17: 138–140.
2. Colquhoun LM, Patrick JW (1997) Pharmacology of neuronal nicotinic acetylcholine receptor subtypes. Adv Pharmacol 39: 191–220.
3. Lewis RJ, Garcia ML (2003) Therapeutic potential of venom peptides. Nat Rev Drug Discov 2: 790–802.
4. Kini RM, Doley R (2010) Structure, function and evolution of three-finger toxins: mini proteins with multiple targets. Toxicon 56: 855–867.
5. Ogawa T, Chijiwa T, Oda-Ueda N, Ohno M (2005) Molecular diversity and accelerated evolution of C-type lectin-like proteins from snake venom. Toxicon 45: 1–14.
6. Kang TS, Georgieva D, Genov N, Murakami MT, Sinha M, et al. (2011) Enzymatic toxins from snake venom: structural characterization and mechanism of catalysis. FEBS J 278: 4544–4576.
7. Pawlak J, Mackessy SP, Fry BG, Bhatia M, Mourier G, et al. (2006) Denmotoxin, a three-finger toxin from the colubrid snake Boiga dendrophila (Mangrove Catsnake) with bird-specific activity. J Biol Chem 281: 29030–29041.
8. Junqueira-de-Azevedo IL, Ching AT, Carvalho E, Faria F, Nishiyama MY, et al. (2006) Lachesis muta (Viperidae) cDNAs reveal diverging pit viper molecules and scaffolds typical of cobra (Elapidae) venoms: implications for snake toxin repertoire evolution. Genetics 173: 877–889.
9. Pahari S, Bickford D, Fry BG, Kini RM (2007) Expression pattern of three-finger toxin and phospholipase A2 genes in the venom glands of two sea snakes, Lapemis curtus and Acalyptophis peronii: comparison of evolution of these toxins in land snakes, sea kraits and sea snakes. BMC Evol Biol 7: 175.
10. Tsetlin V (1999) Snake venom alpha-neurotoxins and other 'three-finger' proteins. Eur J Biochem 264: 281–286.
11. Kini RM (2002) Molecular moulds with multiple missions: functional sites in three-finger toxins. Clin Exp Pharmacol Physiol 29: 815–822.
12. Dufton MJ, Hider RC (1983) Conformational properties of the neurotoxins and cytotoxins isolated from Elapid snake venoms. CRC Crit Rev Biochem 14: 113–171.
13. Nirthanan S, Charpantier E, Gopalakrishnakone P, Gwee MC, Khoo HE, et al. (2003) Neuromuscular effects of candoxin, a novel toxin from the venom of the Malayan krait (Bungarus candidus). Br J Pharmacol 139: 832–844.
14. Oswald RE, Sutcliffe MJ, Bamberger M, Loring RH, Braswell E, et al. (1991) Solution structure of neuronal bungarotoxin determined by two-dimensional NMR spectroscopy: sequence-specific assignments, secondary structure, and dimer formation. Biochemistry 30: 4901–4909.
15. Roy A, Zhou X, Chong MZ, D'hoedt D, Foo CS, et al. (2010) Structural and functional characterization of a novel homodimeric three-finger neurotoxin from the venom of Ophiophagus hannah (king cobra). J Biol Chem 285: 8302–8315.
16. Dewan JC, Grant GA, Sacchettini JC (1994) Crystal structure of kappa-bungarotoxin at 2.3-A resolution. Biochemistry 33: 13147–13154.
17. Grant GA, Al-Rabiee R, Xu XL, Zhang Y (1997) Critical interactions at the dimer interface of kappa-bungarotoxin, a neuronal nicotinic acetylcholine receptor antagonist. Biochemistry 36: 3353–3358.
18. Osipov AV, Kasheverov IE, Makarova YV, Starkov VG, Vorontsova OV, et al. (2008) Naturally occurring disulfide-bound dimers of three-fingered toxins: a paradigm for biological activity diversification. J Biol Chem 283: 14571–14580.
19. Pawlak J, Mackessy SP, Sixberry NM, Stura EA, Le Du MH, et al. (2009) Irditoxin, a novel covalently linked heterodimeric three-finger toxin with high taxon-specific neurotoxicity. FASEB J 23: 534–545.
20. Osipov AV, Rucktooa P, Kasheverov IE, Filkin SY, Starkov VG, et al. (2012) Dimeric α-cobratoxin X-ray structure: localization of intermolecular disulfides and possible mode of binding to nicotinic acetylcholine receptors. J Biol Chem 287: 6725–6734.
21. Ohno M, Ménez R, Ogawa T, Danse JM, Shimohigashi Y, et al. (1998) Molecular evolution of snake toxins: is the functional diversity of snake toxins associated with a mechanism of accelerated evolution? Prog Nucleic Acid Res Mol Biol 59: 307–364.
22. Ricciardi A, le Du MH, Khayati M, Dajas F, Boulain JC, et al. (2000) Do structural deviations between toxins adopting the same fold reflect functional differences? J Biol Chem 275: 18302–18310.
23. Endo T, Tamiya N (1991) Structure-function relationship of postsynaptic neurotoxins from snake venoms. In: Harvey, A.L. (Ed.), Snake Toxins. Pergamon Press, New York, 165–222.
24. Karlsson E, Jolkkonen M, Mulugeta E, Onali P, Adem A (2000) Snake toxins with high selectivity for subtypes of muscarinic acetylcholine receptors. Biochimie 82: 793–806.
25. Dufton MJ, Hider RC (1988) Structure and pharmacology of elapid cytotoxins. Pharmacol Ther 36: 1–40.
26. Eastman J, Wilson EJ, Cerveñansky C, Rosenberry TL (1995) Fasciculin 2 binds to the peripheral site on acetylcholinesterase and inhibits substrate hydrolysis by slowing a step involving proton transfer during enzyme acylation. J Biol Chem 270: 19694–19701.
27. de Weille JR, Schweitz H, Maes P, Tartar A, Lazdunski M (1991) Calciseptine, a peptide isolated from black mamba venom, is a specific blocker of the L-type calcium channel. Proc Natl Acad Sci U S A 88: 2437–2440.
28. Yasuda O, Morimoto S, Jiang B, Kuroda H, Kimura T, et al. (1994) FS2. a mamba venom toxin, is a specific blocker of the L-type calcium channels. Artery 21: 287–302.
29. Rajagopalan N, Pung YF, Zhu YZ, Wong PT, Kumar PP, et al. (2007) Beta-cardiotoxin: a new three-finger toxin from Ophiophagus hannah (king cobra) venom with beta-blocker activity. FASEB J 21: 3685–3695.
30. McDowell RS, Dennis MS, Louie A, Shuster M, Mulkerrin MG, et al. (1992) Mambin, a potent glycoprotein IIb-IIIa antagonist and platelet aggregation inhibitor structurally related to the short neurotoxins. Biochemistry 31: 4766–4772.
31. Wu PL, Lee SC, Chuang CC, Mori S, Akakura N, et al. (2006) Non-cytotoxic cobra cardiotoxin A5 binds to alpha(v)beta3 integrin and inhibits bone resorption. Identification of cardiotoxins as non-RGD integrin-binding proteins of the Ly-6 family. J Biol Chem 281: 7937–7945.
32. Quinton L, Girard E, Maiga A, Rekik M, Lluel P, et al. (2010) Isolation and pharmacological characterization of AdTx1, a natural peptide displaying specific insurmountable antagonism of the alpha1A-adrenoceptor. Br J Pharmacol 159: 316–325.
33. Rouget C, Quinton L, Maïga A, Gales C, Masuyer G, et al. (2010) Identification of a novel snake peptide toxin displaying high affinity and antagonist behaviour for the α2-adrenoceptors. Br J Pharmacol 161: 1361–1374.
34. Kolbe HV, Huber A, Cordier P, Rasmussen UB, Bouchon B, et al. (1993) Xenoxins, a family of peptides from dorsal gland secretion of Xenopus laevis related to snake venom cytotoxins and neurotoxins. J Biol Chem 268: 16458–16464.
35. Nau F, Guérin-Dubiard C, Désert C, Gautron J, Bouton S, et al. (2003) Cloning and characterization of HEP21, a new member of the uPAR/Ly6 protein superfamily predominantly expressed in hen egg white. Poult Sci 82: 242–250.
36. Gumley TP, McKenzie IF, Sandrin MS (1995) Tissue expression, structure and function of the murine Ly-6 family of molecules. Immunol Cell Biol 73: 277–296.
37. Ploug M, Ellis V (1994) Structure-function relationships in the receptor for urokinase-type plasminogen activator. Comparison to other members of the Ly-6 family and snake venom alpha-neurotoxins. FEBS Lett 349: 163–168.
38. Fletcher CM, Harrison RA, Lachmann PJ, Neuhaus D (1994) Structure of a soluble, glycosylated form of the human complement regulatory protein CD59. Structure 2: 185–199.
39. Kordis D, Gubensek F (2000) Adaptive evolution of animal toxin multigene families. Gene 261: 43–52.
40. Zupunski V, Kordis D, Gubensek F (2003) Adaptive evolution in the snake venom Kunitz/BPTI protein family. FEBS Lett 547: 131–136.
41. Hou X, Chen M, Chen L, Meehan EJ, Xie J, et al. (2007) X-ray sequence and crystal structure of luffaculin 1, a novel type 1 ribosome-inactivating protein. BMC Struct Biol 7: 29.
42. Altschul S, Madden T, Schäffer A, Zhang J, Zhang Z, et al. (1997) Gapped BLAST and PSI-BLAST: a new generation of protein database search programs. Nucleic Acids Res 25: 3389–3402.
43. Fryklund L, Eaker D (1973) Complete amino acid sequence of a nonneurotoxic hemolytic protein from the venom of Haemachatus haemachates (African ringhals cobra). Biochemistry 12: 661–667.
44. Joubert FJ (1977) Snake venom toxins. The amino-acid sequences of three toxins (9B, 11 and 12A) from Hemachatus haemachatus (Ringhals) venom. Eur J Biochem 74: 387–396.
45. Laskowski R, Moss D, Thornton J (1993) Main-chain bond lengths and bond angles in protein structures. J Mol Biol 231: 1049–1067.
46. Holm L, Sander C (1998) Touring protein fold space with Dali/FSSP. Nucleic Acids Res 26: 316–319.

47. Corfield PW, Lee TJ, Low BW (1989) The crystal structure of erabutoxin a at 2.0-A resolution. J Biol Chem 264: 9239–9242.
48. Love RA, Stroud RM (1986) The crystal structure of alpha-bungarotoxin at 2.5 A resolution: relation to solution structure and binding to acetylcholine receptor. Protein Eng 1: 37–46.
49. Sun YJ, Wu WG, Chiang CM, Hsin AY, Hsiao CD (1997) Crystal structure of cardiotoxin V from Taiwan cobra venom: pH-dependent conformational change and a novel membrane-binding motif identified in the three-finger loops of P-type cardiotoxin. Biochemistry 36: 2403–2413.
50. Wang CH, Liu JH, Lee SC, Hsiao CD, Wu WG (2006) Glycosphingolipid-facilitated membrane insertion and internalization of cobra cardiotoxin. The sulfatide.cardiotoxin complex structure in a membrane-like environment suggests a lipid-dependent cell-penetrating mechanism for membrane binding polypeptides. J Biol Chem 281: 656–667.
51. Forouhar F, Huang WN, Liu JH, Chien KY, Wu WG, et al. (2003) Structural basis of membrane-induced cardiotoxin A3 oligomerization. J Biol Chem 278: 21980–21988.
52. Bilwes A, Rees B, Moras D, Ménez R, Ménez A (1994) X-ray structure at 1.55 A of toxin gamma, a cardiotoxin from Naja nigricollis venom. Crystal packing reveals a model for insertion into membranes. J Mol Biol 239: 122–136.
53. Carsi JM, Potter LT (2000) m1-toxin isotoxins from the green mamba (Dendroaspis angusticeps) that selectively block m1 muscarinic receptors. Toxicon 38: 187–198.
54. Fernández J, Alape-Girón A, Angulo Y, Sanz L, Gutiérrez JM, et al. (2011) Venomic and antivenomic analyses of the Central American coral snake, Micrurus nigrocinctus (Elapidae). J Proteome Res 10: 1816–1827.
55. Ruan KH, Stiles BG, Atassi MZ (1991) The short-neurotoxin-binding regions on the alpha-chain of human and Torpedo californica acetylcholine receptors. Biochem J 274 (Pt 3): 849–854.
56. Teixeira-Clerc F, Ménez A, Kessler P (2002) How do short neurotoxins bind to a muscular-type nicotinic acetylcholine receptor? J Biol Chem 277: 25741–25747.
57. Antil S, Servent D, Ménez A (1999) Variability among the sites by which curaremimetic toxins bind to torpedo acetylcholine receptor, as revealed by identification of the functional residues of alpha-cobratoxin. J Biol Chem 274: 34851–34858.
58. Servent D, Antil-Delbeke S, Gaillard C, Corringer PJ, Changeux JP, et al. (2000) Molecular characterization of the specificity of interactions of various neurotoxins on two distinct nicotinic acetylcholine receptors. Eur J Pharmacol 393: 197–204.
59. Rosenthal JA, Levandoski MM, Chang B, Potts JF, Shi QL, et al. (1999) The functional role of positively charged amino acid side chains in alpha-bungarotoxin revealed by site-directed mutagenesis of a His-tagged recombinant alpha-bungarotoxin. Biochemistry 38: 7847–7855.
60. Fruchart-Gaillard C, Gilquin B, Antil-Delbeke S, Le Novère N, Tamiya T, et al. (2002) Experimentally based model of a complex between a snake toxin and the alpha 7 nicotinic receptor. Proc Natl Acad Sci U S A 99: 3216–3221.
61. Servent D, Winckler-Dietrich V, Hu HY, Kessler P, Drevet P, et al. (1997) Only snake curaremimetic toxins with a fifth disulfide bond have high affinity for the neuronal alpha7 nicotinic receptor. J Biol Chem 272: 24279–24286.
62. Antil-Delbeke S, Gaillard C, Tamiya T, Corringer PJ, Changeux JP, et al. (2000) Molecular determinants by which a long chain toxin from snake venom interacts with the neuronal alpha 7-nicotinic acetylcholine receptor. J Biol Chem 275: 29594–29601.
63. Bourne Y, Talley TT, Hansen SB, Taylor P, Marchot P (2005) Crystal structure of a Cbtx-AChBP complex reveals essential interactions between snake alpha-neurotoxins and nicotinic receptors. EMBO J 24: 1512–1522.
64. Harel M, Kleywegt GJ, Ravelli RB, Silman I, Sussman JL (1995) Crystal structure of an acetylcholinesterase-fasciculin complex: interaction of a three-fingered toxin from snake venom with its target. Structure 3: 1355–1366.
65. Albrand JP, Blackledge MJ, Pascaud F, Hollecker M, Marion D (1995) NMR and restrained molecular dynamics study of the three-dimensional solution structure of toxin FS2, a specific blocker of the L-type calcium channel, isolated from black mamba venom. Biochemistry 34: 5923–5937.
66. Sutcliffe MJ, Jaseja M, Hyde EI, Lu X, Williams JA (1994) Three-dimensional structure of the RGD-containing neurotoxin homologue dendroaspin. Nat Struct Biol 1: 802–807.
67. Chien KY, Chiang CM, Hseu YC, Vyas AA, Rule GS, et al. (1994) Two distinct types of cardiotoxin as revealed by the structure and activity relationship of their interaction with zwitterionic phospholipid dispersions. J Biol Chem 269: 14473–14483.
68. Dubovskii PV, Dementieva DV, Bocharov EV, Utkin YN, Arseniev AS (2001) Membrane binding motif of the P-type cardiotoxin. J Mol Biol 305: 137–149.
69. Dubovskii PV, Lesovoy DM, Dubinnyi MA, Utkin YN, Arseniev AS (2003) Interaction of the P-type cardiotoxin with phospholipid membranes. Eur J Biochem 270: 2038–2046.
70. Kini RM, Evans HJ (1989) A common cytolytic region in myotoxins, hemolysins, cardiotoxins and antibacterial peptides. Int J Pept Protein Res 34: 277–286.
71. Kini RM, Evans HJ (1989) Role of cationic residues in cytolytic activity: modification of lysine residues in the cardiotoxin from Naja nigricollis venom and correlation between cytolytic and antiplatelet activity. Biochemistry 28: 9209–9215.
72. Joseph JS, Chung MC, Jeyaseelan K, Kini RM (1999) Amino acid sequence of trocarin, a prothrombin activator from Tropidechis carinatus venom: its structural similarity to coagulation factor Xa. Blood 94: 621–631.
73. Otwinowski Z, Minor W (1997) Processing of X-ray diffraction data collected in oscillation mode. Methods in enzymology: Academic press. 307–326.
74. McCoy A (2007) Solving structures of protein complexes by molecular replacement with Phaser. Acta Crystallogr D Biol Crystallogr 63: 32–41.
75. Emsley P, Cowtan K (2004) Coot: model-building tools for molecular graphics. Acta Crystallogr D Biol Crystallogr 60: 2126–2132.
76. Adams PD, Afonine PV, Bunkóczi G, Chen VB, Davis IW, et al. (2010) PHENIX: a comprehensive Python-based system for macromolecular structure solution. Acta Crystallogr D Biol Crystallogr 66: 213–221.
77. Delano WL (2002) The PyMOL molecular graphics system.
78. Larkin M, Blackshields G, Brown N, Chenna R, McGettigan P, et al. (2007) Clustal W and Clustal X version 2.0. Bioinformatics 23: 2947–2948.
79. Gouet P, Courcelle E, Stuart D, Métoz F (1999) ESPript: analysis of multiple sequence alignments in PostScript. Bioinformatics 15: 305–308.
80. Lee SC, Guan HH, Wang CH, Huang WN, Tjong SC, et al. (2005) Structural basis of citrate-dependent and heparan sulfate-mediated cell surface retention of cobra cardiotoxin A3. J Biol Chem 280: 9567–9577.
81. Chen TS, Chung FY, Tjong SC, Goh KS, Huang WN, et al. (2005) Structural difference between group I and group II cobra cardiotoxins: X-ray, NMR, and CD analysis of the effect of cis-proline conformation on three-fingered toxins. Biochemistry 44: 7414–7426.
82. Rees B, Bilwes A, Samama JP, Moras D (1990) Cardiotoxin VII4 from Naja mossambica mossambica. The refined crystal structure. J Mol Biol 214: 281–297.
83. Dementieva DV, Bocharov EV, Arseniev AS (1999) Two forms of cytotoxin II (cardiotoxin) from Naja naja oxiana in aqueous solution: spatial structures with tightly bound water molecules. Eur J Biochem 263: 152–162.
84. Fruchart-Gaillard C, Mourier G, Marquer C, Stura E, Birdsall NJ, et al. (2008) Different interactions between MT7 toxin and the human muscarinic M1 receptor in its free and N-methylscopolamine-occupied states. Mol Pharmacol 74: 1554–1563.
85. Dellisanti CD, Yao Y, Stroud JC, Wang ZZ, Chen L (2007) Crystal structure of the extracellular domain of nAChR alpha1 bound to alpha-bungarotoxin at 1.94 A resolution. Nat Neurosci 10: 953–962.
86. Gaucher JF, Ménez R, Arnoux B, Pusset J, Ducruix A (2000) High resolution x-ray analysis of two mutants of a curaremimetic snake toxin. Eur J Biochem 267: 1323–1329.
87. le Du MH, Housset D, Marchot P, Bougis PE, Navaza J, et al. (1996) Structure of fasciculin 2 from green mamba snake venom: evidence for unusual loop flexibility. Acta Crystallogr D Biol Crystallogr 52: 87–92.